Fluorine Route Synthesis of Montmorillonites Containing Mg or Zn and Characterization by XRD, Thermal Analysis, MAS NMR, and EXAFS Spectroscopy

Marc Reinholdt,*[a,b] Jocelyne Miehé-Brendlé,[a] Luc Delmotte,[a] Marie-Hélène Tuilier,[b] Ronan le Dred,[a] Robert Cortès,[c] and Anne-Marie Flank[c]

Keywords: Montmorillonite / Clays / Synthesis / Fluorine / Solid-state NMR / EXAFS spectroscopy

EXAFS spectroscopy, combined with X-ray powder diffraction, chemical and thermal analysis, scanning electronic microscopy, ^{29}Si, ^{27}Al, and ^{19}F MAS NMR spectroscopy, are used in the structural analysis of montmorillonites, synthesised in an acidic fluoride medium. Hydrothermal synthesis performed under mild conditions (493 K, autogenous pressure) enables the formation of montmorillonite clays, containing Al and Zn or Mg in the octahedral sheet. It is shown that montmorillonites can only be synthesized in a narrow range of compositions. An accurate value of the Al for Si substitution rate in the tetrahedral sheet is determined by using ^{27}Al MAS NMR spectroscopy performed under definite conditions. Some interatomic distances are determined by EXAFS spectroscopy (R_{Mg-O} = 2.11 Å, R_{Zn-O} = 2.08 Å, R_{Zn-Al} = 2.98 Å, R_{Zn-Zn} = 3.11 Å) which reveals strong local distortions in the octahedral sheet with respect to the ideal montmorillonite structure. Lengthening of the out-of-plane Zn–Si(Al) distances also shows the swelling of the whole layer in the neighbourhood of Zn. Moreover, the combination of EXAFS and ^{19}F MAS NMR spectroscopic data reveals a clustering of the divalent elements of the octahedral sheet, which is related to a possible local trioctahedral character of these materials.

Introduction

Smectites present in soils and sediments are one of the largest and most important classes of the phyllosilicate clay minerals group. Their ability to swell upon contact with water and other solvents is extensively used in two fields of application. The first one is related to the properties of adsorption (use in the selective adsorption of toxic compounds from water, detergents, organic chemistry, etc.).[1] The other one concerns pillared clays which are commonly used in the field of catalysis.[2,3] The 2:1 structure of smectites consists of two sheets of distorted SiO_4 tetrahedra connected by a sheet of $Al(M)(OH)_2O_4$ octahedra, M being a divalent element (Figure 1a). The silicon and metal atoms occupy the centre of the tetrahedra or the octahedra, with the oxygen atoms and hydroxy groups (OH) located at the corners. Smectites are divided into two groups: the dioctahedral smectites for which the octahedral sheet contains two Al(M) elements in the centre of two out of three octahedra, the third one being vacant; and the trioctahedral smectites which contain only divalent elements in the octahedral sheet without vacancies. Montmorillonite, which belongs to the former group, has been extensively studied. Among the dioctahedral smectites, the distinctive feature of montmorillonite is that transition elements are included in the octahedral sheet whereas Al can be split into the tetrahedral (Al_{IV}) and octahedral (Al_{VI}) sheets. The Al atoms are partially replaced by either Mg or Fe atoms, thereby creating a charge deficiency within the unit structure. This results in a small negative charge on the basal plane of the silica tetrahedra which is balanced by exchangeable cations present in the interlayer spacing. In natural montmorillonites these cations are usually calcium or sodium according to the weather agent associated with the formation of the mineral. The crystal structure of montmorillonite has a *C*2*mm* symmetry.

The ideal formula per half a unit cell, without tetrahedral substitution, is $R_{2x}(Al_{2(1-x)}M_{2x}\ \square)Si_4O_{10}(OH)_2$, where R represents the interlayer cations and x the layer charge ranging from 0.05 to 0.54. Natural montmorillonites usually present isomorphic substitutions in both tetrahedral and octahedral layers. Moreover, depending on the deposits, various structural compositions and particle sizes can be found. These drawbacks, combined with the presence of impurities, limit their use in some applications. One way to avoid these disadvantages is to synthesize such compounds; this enables the control of the chemical composition by fine tuning the preparative methods. Many studies have been performed in this field, as recently mentioned by Kloprogge et al., but only four papers mentioned the synthesis of pure montmorillonite.[4] The first one, by Otsubo and Kato, described Zn for Al partially substituted montmorillonite in the $ZnO-Al_2O_3-SiO_2$ system,[5] the Zn and Al atoms being located in the octahedral sheet and the Si atoms in the tetrahedral sheet. The clay has been prepared under hydrothermal conditions in an alkali medium at temperatures

[a] Laboratoire des Matériaux Minéraux, UPRES-A 7016, 3 rue A. Werner, 68093 Mulhouse Cedex, France
[b] Laboratoire de Physique et Spectroscopie Electronique, UPRES-A 7014, 4 rue des Frères Lumière, 68093 Mulhouse Cedex, France
[c] Laboratoire pour l'Utilisation du Rayonnement Electromagnétique (LURE), Bât 209D, Centre Universitaire, B. P. 34, 91898 Orsay Cedex, France

  1434–1948/01/1111–2831 $ 17.50+.50/0

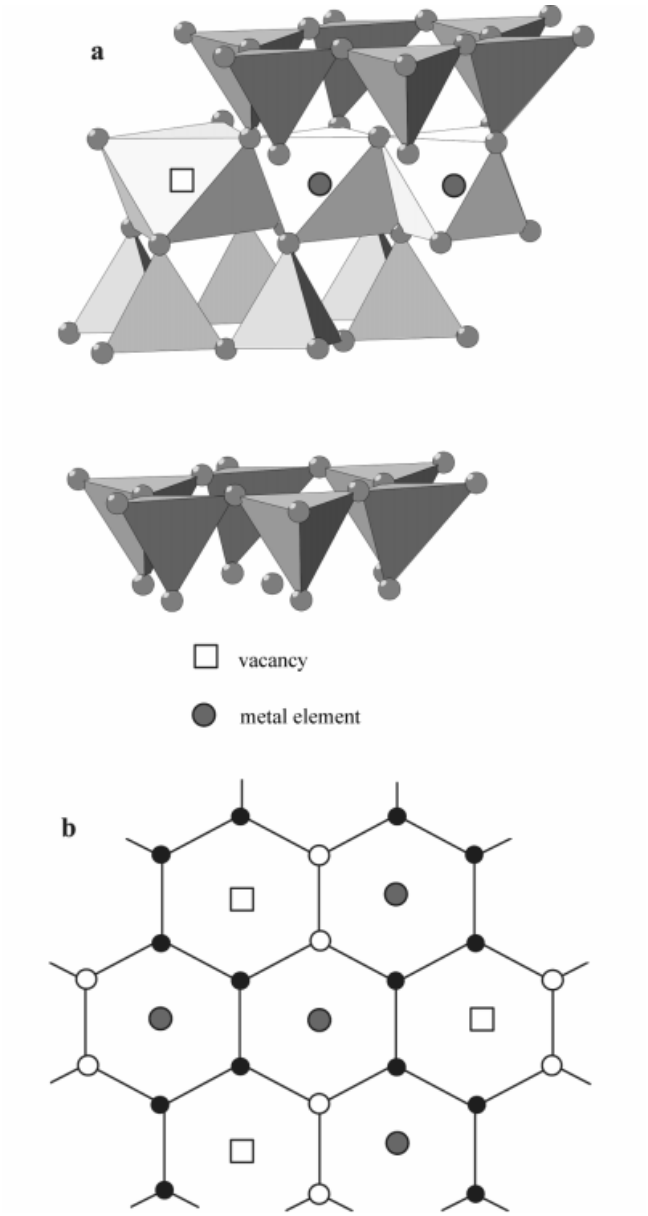

Figure 1. Layer of a 2:1 phyllosilicate (a) and hexagonal cavities (b) of the octahedral sheet of a 2:1 phyllosilicate

ranging from 423 to 573 K, over 5 to 20 h. The second synthesis, described by Harder, was carried out on the basis of the precipitation of hydroxides, in the $MgO-Al_2O_3-SiO_2$ system in an alkali to neutral medium at 276 and 293 K.[6] The same system was studied by Nakazawa et al., but syntheses were performed on magnesium aluminosilicate glass under a hydrothermal pressure of 100 Mpa.[7] A more recent work was also performed in an alkali medium, by Nagase et al., in the $MgO-Fe_2O_3-SiO_2$ system under hydrothermal conditions at 373 and 473 K for 24 h.[8] Samples were characterised by X-ray diffraction (XRD), thermal and chemical analyses, electronic microscopy, or X-ray photoelectron spectroscopy (XPS). None of these studies have brought any information about the distribution of the elements in the structure and their local environment.

The present paper deals with the synthesis of montmorillonites in the $MgO-Al_2O_3-SiO_2$ and $ZnO-Al_2O_3-SiO_2$ systems. Starting from the previously mentioned ideal formula per half a unit cell, we introduced an increasing amount of divalent element (x ranging from 0 to 1) in the hydrogel in order to establish the best conditions to obtain montmorillonite. Samples were labelled Mg($10 \times x$) or Zn($10 \times x$) (Table 1). Syntheses were performed in acidic and fluoride media. Similarly, mild conditions were previously used for the preparation of dioctahedral smectites, such as beidellite,[9,10] and trioctahedral smectites, such as stevensite.[11] In the present work, samples were characterised by XRD, thermal, and chemical analyses. Some of them were selected for further structural investigation by solid-state nuclear magnetic resonance spectroscopy (NMR) and X-ray absorption spectroscopy (XAS), in order to study the local environment of the metallic elements. An explanation of the process of formation of montmorillonite is suggested.

Table 1. Labels of the samples

Sample[a]	x	Theoretical formula[b]
M01	0.1	$Na_{0.2}(Al_{1.8}M_{0.2}\,\square)Si_4O_{10}(OH)_2$
M02	0.2	$Na_{0.4}(Al_{1.6}M_{0.4}\,\square)Si_4O_{10}(OH)_2$
M03	0.3	$Na_{0.6}(Al_{1.4}M_{0.6}\,\square)Si_4O_{10}(OH)_2$
M04	0.4	$Na_{0.8}(Al_{1.2}M_{0.8}\,\square)Si_4O_{10}(OH)_2$
M05	0.5	$Na_{1.0}(Al_{1.0}M_{1.0}\,\square)Si_4O_{10}(OH)_2$
M06	0.6	$Na_{1.2}(Al_{0.8}M_{1.2}\,\square)Si_4O_{10}(OH)_2$
M07	0.7	$Na_{1.4}(Al_{0.6}M_{1.4}\,\square)Si_4O_{10}(OH)_2$
M08	0.8	$Na_{1.6}(Al_{0.4}M_{1.6}\,\square)Si_4O_{10}(OH)_2$
M09	0.9	$Na_{1.8}(Al_{0.2}M_{1.8}\,\square)Si_4O_{10}(OH)_2$
M10	1.0	$Na_{2.0}(M_{2.0}\,\square)Si_4O_{10}(OH)_2$

[a] M represents Mg or Zn. – [b] □ Represents the vacancy.

Results

X-ray Powder Diffraction

XRD patterns of the two series of samples are characteristic of clays (Figure 2). Each diffractogram exhibits *hkl* bands at 4.45–4.48 Å (020, 110), 2.52–2.58 Å (130, 200) and 1.67–1.70 Å (210), which are typical features of smectites.[12] One or two peaks are also observed between 1.48 and 1.53 Å; they correspond to the (060) and (330) reflections. Their relative intensity is related to the dioctahedral (peak at about 1.49 Å) or trioctahedral (peak at about 1.52 Å) nature of the product, i.e. a dioctahedral compound has vacancies in the octahedral sheet and a trioctahedral one has none. The position of the (001) peak gives information about the basal spacing (d_{001}). The basal spacing is equal to the sum of the interlayer spacing and the thickness of the silicate layer, which is about 9.6 Å for a 2:1 phyllosilicate. The usual value of d_{001} is about 15 Å for natural montmorillonites under a relative humidity of $P/P_0 = 80\%$ (P represents the saturated vapour pressure over the sample at 298 K and P_0 the saturated aqueous vapour pressure at 298 K).

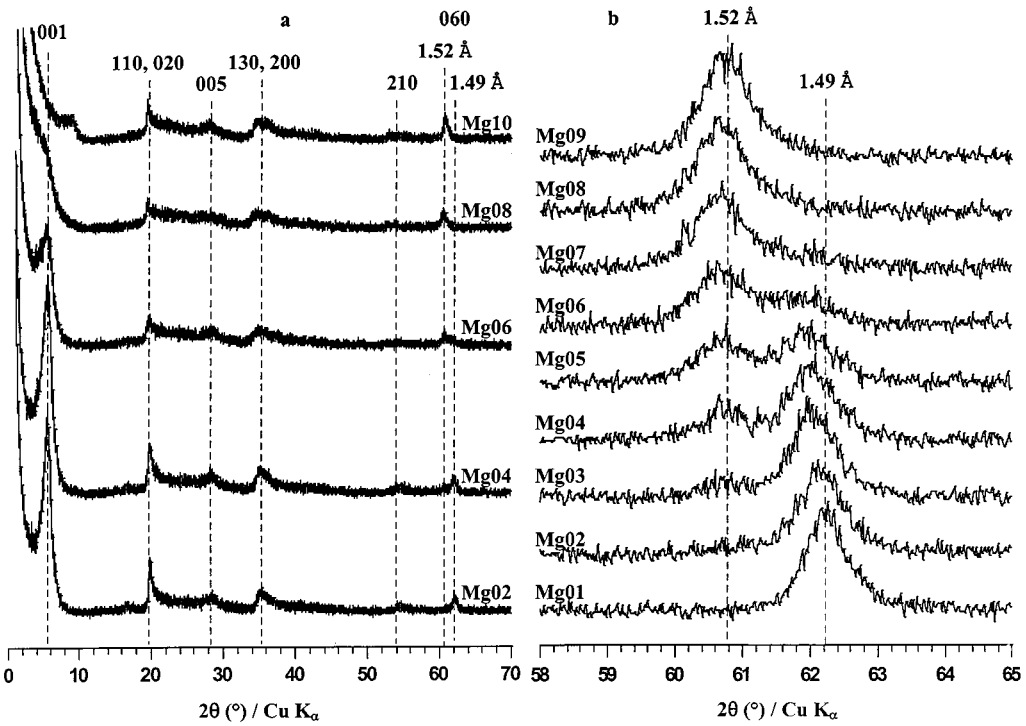

Figure 2. Comparison of the XRD patterns of synthetic clays containing various amount of Mg (P/P_0 = 80%) (a) and evolution of the position of the (060) peak with this amount (b)

A sample which has $x = 0.0$ is unambiguously identified as kaolinite (DRX and TGA-DTA). The Mg01 sample is a dioctahedral clay (d_{060} = 1.49±0.01 Å, Table 2) and the Mg02 sample could have a small trioctahedral component (see next section). Samples Mg03 to Mg06 are mixtures of di- and trioctahedral compounds. Their XRD patterns present two (060) bands, one at 1.49±0.01 Å and a second at 1.52±0.01 Å. For samples Mg07 to Mg09, d_{060} is equal to 1.52±0.01 Å. This value corresponds to trioctahedral compounds. The Mg10 sample is identified as a talc-type clay (probably stevensite) which is trioctahedral, with silicon in the tetrahedral sheet and magnesium in the octahedral sheet. The (001) peak is observed for each sample, except Mg08 and Mg09. This is characteristic of a higher disorder and a lower crystallinity of the samples. The Zn01 sample has the position of the (060) peak corresponding to a dioctahedral compound (d_{060} = 1.49±0.01 Å, Table 2). The Zn02 sample could have a little trioctahedral component (see next section). Similarly to the Mg series, the Zn03 to Zn06 samples are mixtures of di- and trioctahedral clays and the Zn07 to Zn09 samples have the structure of trioctahedral compounds (d_{060} = 1.52±0.01 Å). Each diffractogram of Zn(10 × x) samples exhibits a (001) peak, contrary to some of the Mg(10 × x) samples. The Zn10 sample is identified as a mixture of an amorphous phase and willemite (Zn_2SiO_4). The investigation of samples containing a mixture of clays was not carried out beyond this preliminary characterisation. Trioctahedral products are also dismissed because of the presence of amorphous silica, observed by NMR spectroscopy (see the paragraph about solid-state NMR spectroscopy). Consequently, only the Mg01, Mg02, Zn01, and Zn02 samples will be further characterised. Their diffractograms exhibit the characteristic *hk* bands of montmorillonite.[12] The position of the (060) peak indicates the dioctahedral nature of the sample, i.e. the presence of vacancies in the octahedral sheet, except for the Mg02 and Zn02 samples, which can have a weak trioctahedral component at 1.52 Å (Figures 2 and 3 and discussion section). As a comparison, Figure 3 (inset) shows the diffractogram of a natural clay from Camp Berteau which contains quartz. The study of the (001) peak position was performed on samples which were previously placed under a controlled humidity (P/P_0 = 80%). The d_{001} values are listed in Table 2. These values are in good agreement with those indexed in the literature for natural Na-exchanged montmorillonites (d_{001} = 15−16 Å).[13−15] The (001) peaks are more symmetrical and intense than they are for samples containing Mg.

Scanning Electronic Microscopy

The micrographs of the Mg01 sample are presented in Figure 4. The picture shows crumpled platelets that look like gypsum flower. More compact aggregates are also observed. Natural montmorillonites present this typical morphology.[16−18] The samples of Mg01, Zn01, and Zn02 have a similar morphology.

Table 2. X-ray diffraction, and thermal analysis data of samples Mg01, Mg02, Zn01, and Zn02

Sample	XRD		TGA-DTA[a]		
	d_{001} [A]	d_{060} [A]	Dehydration [K]	Dehydroxylation [K] First peak	Second peak
Mg01	16.5	1.49	350	750	930
Mg02	16.1	1.49	360	–	930
Zn01	17.4	1.49	360	750	950
Zn02	16.4	1.49	365	730	940

[a] Temperatures are taken at the inflexion point of the weight losses on the TGA curves.

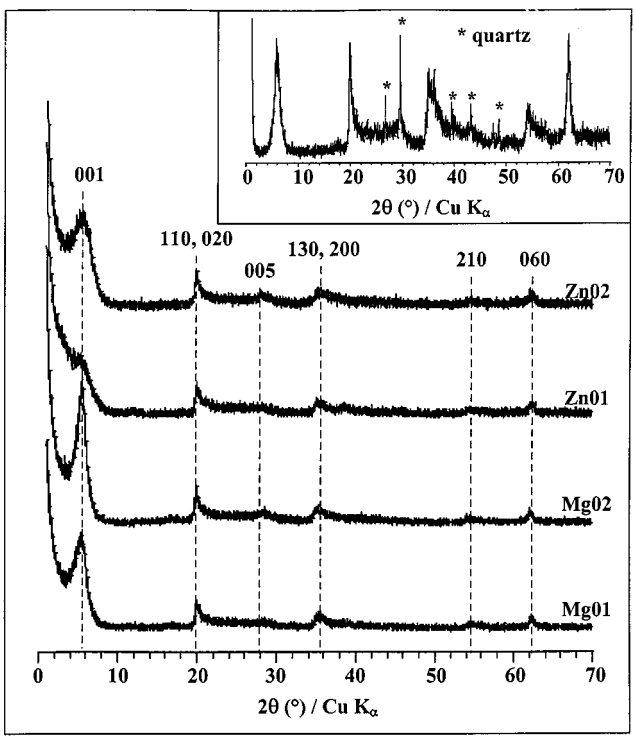

Figure 3. XRD patterns of synthetic montmorillonites containing Mg or Zn (P/P_0 = 80%); inset: diffractogram of natural montmorillonite from Camp Berteau

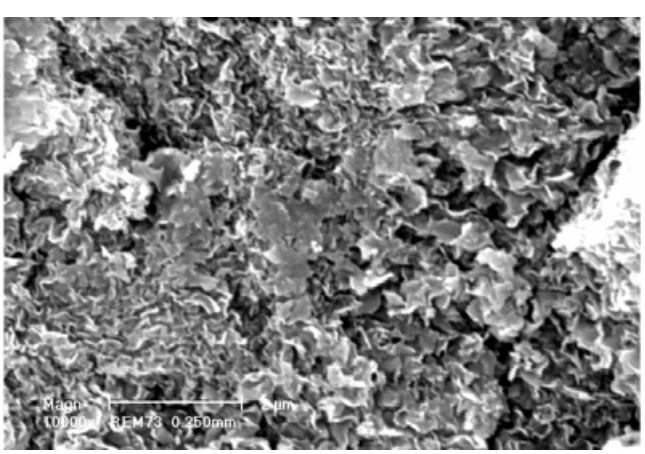

Figure 4. SEM micrograph of Zn02 sample

TGA-DTA

The curves of weight loss and heat flow versus temperature are shown in Figure 5. Each sample exhibits a main peak at 370 K corresponding to dehydration. Moreover, the Mg01, Zn01, and Zn02 samples exhibit two peaks, at about 720−760 K and 920−960 K, which are attributed to the dehydroxylation. The peaks of dehydroxylation are observed at 750 and 930 K for the Mg01 sample, 750 and 950 K for the Zn01 sample, and 730 and 930 K for the Zn02 sample (Figure 5). In the case of the Mg02 sample, only one dehydroxylation peak is observed at 930 K. The peak ranging from 920 to 960 K was already reported in the literature.[19−23] It is characteristic of natural montmorillonites. The peak ranging from 720 to 760 K was observed by Cuadros et al.[20] on DTA curves of samples coming from the deposit of "Los Trancos" in Almeria (SE Spain) and by Frost et al.[23] on ferruginous montmorillonite SWa-1 (Clay Mineral Society standard).

Chemical Analysis

The results of elemental analyses are listed in Table 3. Na and divalent element contents are higher, whereas the Al content is lower, in samples of Mg02 and Zn02 than in the Mg01 and Zn01 samples. The content of divalent element has roughly doubled in Mg02 (Zn02) with respect to Mg01 (Zn01). This is in good agreement with the theoretical compositions. It should be noted that there is a small amount of fluorine in each sample, so this element could only be considered as a local probe. The half unit cell formula was calculated for the four selected samples (last column of Table 3) on the basis of twenty two negative charges of the layer. However, chemical analysis does not enable one to determine whether Al is only in the octahedral sheet or if there is some Al in the tetrahedral sheet.

Solid-State NMR Spectroscopy

^{29}Si NMR spectroscopy, using the magic-angle spinning technique (^{29}Si MAS NMR), gives information on the Al-for-Si substitution in the tetrahedral sheet. In the case of trioctahedral products, the presence of a small quantity of amorphous silica was revealed by ^{29}Si MAS NMR spectroscopy. The ^{29}Si MAS NMR spectra of Mg01, Mg02, Zn01, and Zn02 samples (Figure 6) show signals corresponding to Si(nAl) (n ranges from 0 to 3) environments where n represents the number of tetrahedral Al atoms that are next-nearest neighbours of Si. The main peak, which appears at a chemical shift (δ) of $\delta \approx -93$ is assigned to the Si(0Al) environment, i.e. Si surrounded by three Si in the tetrahedral sheet.[24,25] The shoulder observed at $\delta \approx -90$ is attributed to the Si(1Al) environment, i.e. Si surrounded by one Al and two Si in the tetrahedral sheet. The presence of these signals indicates that Al is substituted for Si in the tetrahedral sheet, which could not be observed by chemical analysis. The shielding of the Si(0Al) site increases with the amount of Mg. The same behaviour is observed for the Zn01 and Zn02 samples but with an enhanced effect. These phenomena can be correlated to the increase of the average

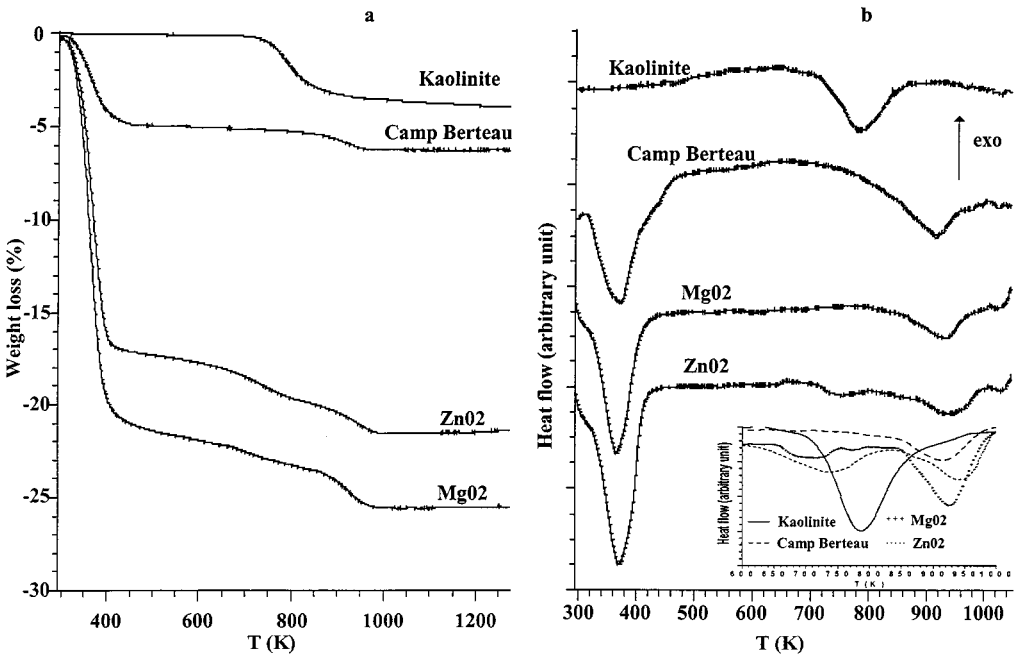

Figure 5. TG patterns of natural and synthetic clays (a) and ATD curves of the same samples (b); inset: comparison of the dehydroxylation peaks of each sample between 600 to 1000 K

Table 3. Half a unit cell formula calculated from chemical analysis for samples Mg01, Mg02, Zn01, and Zn02

Sample	Elemental analyses (mass-%)								Half a unit cell formula[a]
	Na_2O	MgO	ZnO	Al_2O_3	SiO_2	F	H_2O	sum	
Mg01	2.03	1.63	–	22.53	55.54	0.23	17.90	99.86	$Na_{0.28}[Al_{1.81}Mg_{0.18}\,\square_{1.01}]$-$[Si_{3.93}Al_{0.07}]O_{10}(OH_{1.95}F_{0.05})\cdot 3.3H_2O$
Mg02	2.34	3.40	–	19.02	55.00	0.20	19.95	99.91	$Na_{0.34}[Al_{1.64}Mg_{0.37}\,\square_{0.99}]$-$[Si_{4.00}]O_{10}(OH_{1.95}F_{0.05})\cdot 4.0H_2O$
Zn01	1.36	–	3.21	22.21	57.58	0.28	15.77	100.41	$Na_{0.17}[Al_{1.83}Zn_{0.17}\,\square_{1.00}]$-$[Si_{4.00}]O_{10}(OH_{1.94}F_{0.06})\cdot 2.8H_2O$
Zn02	1.98	–	6.90	18.30	55.70	0.20	19.25	102.33	$Na_{0.3}[Al_{1.64}Zn_{0.39}\,\square_{0.97}]$-$[Si_{4.00}]O_{10}(OH_{1.95}F_{0.05})\cdot 4.0H_2O$

[a] □ Represents the vacancy.

Si−O−Si bond angle[26] that was previously observed by Sanz and Serratosa.[24]

^{19}F MAS NMR spectroscopy confirms the substitution of fluoride ions for hydroxy groups, and reveals their environment.[11,27] Spectra (Figure 7) show several peaks with chemical shifts corresponding to various fluorine environments. In the spectrum of the Mg01 sample, two peaks are observed at δ = −133.3 and −153.0 which correspond to Al−Al−□ and Mg−Al−□ fluorine environments, respectively (□ represents a vacancy in the octahedral sheet). For the spectrum of the Mg02 sample, only the Mg−Al−□ peak is conserved at δ = −153.0 and another appears at δ = −177.0 which is characteristic of an Mg−Mg−Mg fluorine environment. The latter was previously observed for trioctahedral compounds like natural hectorite and synthetic mica-montmorillonite clay.[27] The two chemical shifts in the Zn01 and Zn02 samples are assigned to Al−Al−□ (δ = −132.8) and Zn−Al−□ (δ = −142.0 for Zn01 and δ = −142.4 for Zn02) fluorine sites, respectively.[11] The intensity of the former decreases whereas that of the latter increases as the Zn content increases. Consequently, ^{19}F MAS NMR spectroscopy shows the presence of Mg or Zn in the octahedral sheet and the presence of vacancies in the octahedral sheet.

^{27}Al MAS NMR spectroscopy indicates the localisation of Al in the structure.[24,28] The presence of Al_{VI} (δ = 2−3) and Al_{IV} (δ = 64−67) aluminium is observed in the structure (Figure 8). This is further proof for the Al-for-Si substitution in the tetrahedral sheet. The chemical shifts of Al_{VI} and Al_{IV} increase with the content of divalent element.

X-ray Absorption Spectroscopy (XAS)

The Zn *k*-edge extended X-ray absorption fine structure (EXAFS) spectra recorded from Zn01 and Zn02 montmorillonites are shown in Figure 9a, after background subtraction and conversion to *k*-space. There are no major differences between the data except for a slight enhancement of

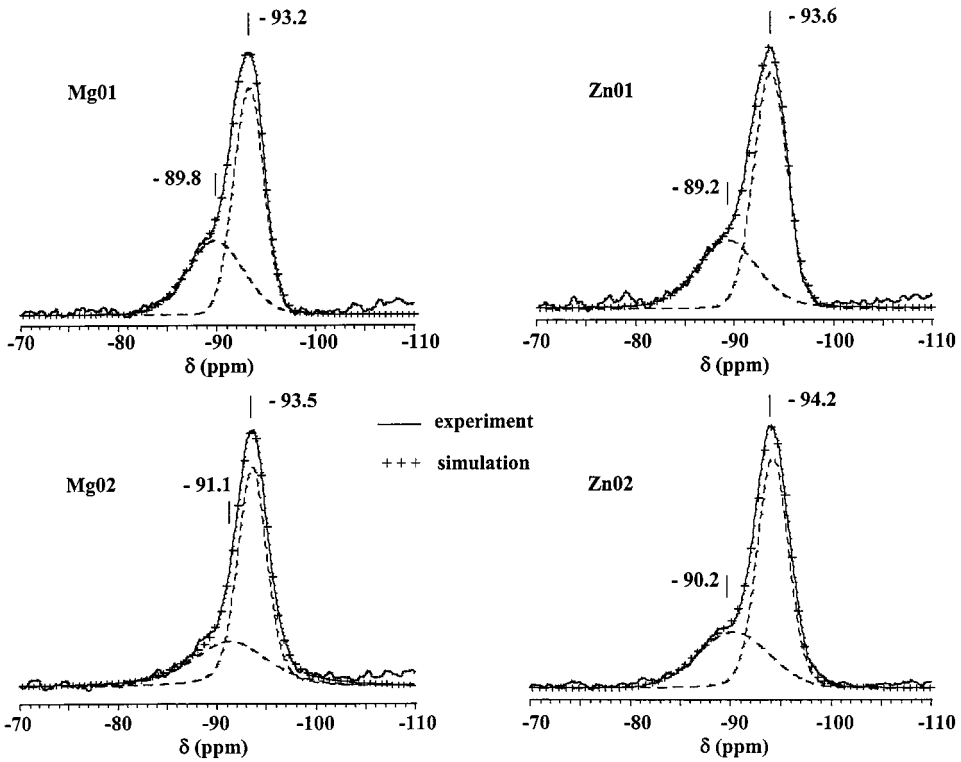

Figure 6. ^{29}Si MAS NMR spectra [standard reference $Si(CH_3)_4$] and corresponding simulations of the studied synthetic montmorillonites

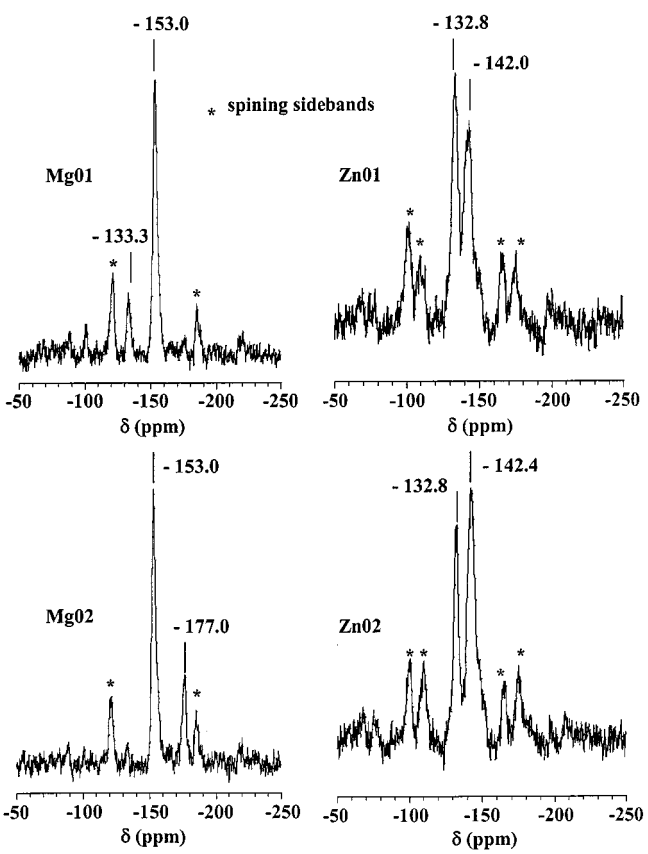

Figure 7. ^{19}F MAS NMR spectra of samples Mg01, Mg02, Zn01, and Zn02 (standard reference $CFCl_3$)

the high frequency oscillation for Zn02. The corresponding Fourier transforms (FT) between 0 and 8 Å are presented in Figure 9b. The main peak, which is assigned to the oxygen atom's nearest neighbours (NN), has the same position and amplitude for both samples. The structural parameters, derived from the simulation of the Fourier-filtered contribution of the NN peak, are reported in Table 4. Figure 10a compares the experimental and calculated curves. Zn is formed in octahedral coordination with O in agreement with the other characterisations; the average bond length is found to be 2.08 Å. The second and third peaks observed between 2 and 3.5 Å in FT (Figure 9 b) are not well separated and are related to Al and Zn next-nearest neighbours (NNN) in the octahedral sheet on one hand, and Si(Al) belonging to the tetrahedral sheets on the other hand. Some preliminary considerations have to be made before giving the results of the simulations. In the ideal montmorillonite lattice, the shortest metal−metal distance within the octahedral sheet is 2.99 Å, whereas the distance from sixfold-coordinated metal to fourfold-coordinated Si(Al) is 3.11−3.18 Å.[29] On the other hand, the average number of metallic neighbours inside the octahedral sheet is assumed to be four from the rate of vacancies (see next section), whereas the number of Si(Al) neighbours remains equal to 4 (2 per tetrahedral sheet) as in the theoretical structure. The Fourier-filtered contributions of the 2−3.5 Å region in FT are presented in Figure 10b, together with their best fits using the structural parameters of Table 4. They exhibit strong differences in the low *k*-range, which involves mainly Al and Si backscatterers. Indeed it is well known that Al's and Si's backscattering (BS) amplitudes, which are very

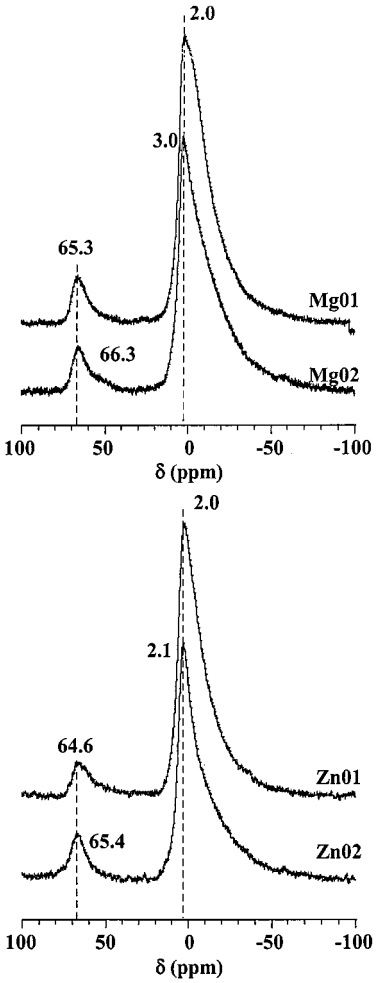

Figure 8. ^{27}Al MAS NMR spectra [standard reference $Al(H_2O)_6^{3+}$] of the studied synthetic montmorillonites

close together, present a maximum around 3−4 $Å^{-1}$ and are strongly dampened above 9−10 $Å^{-1}$ (ref.[30] and references therein). The behaviour of the Zn BS amplitude is quite different, with a minimum at low k and a maximum around 8−9 $Å^{-1}$. Therefore the high k-range of the data (Figure 10b) involves the Zn neighbours of Zn almost exclusively. The positions of the oscillations above 8 $Å^{-1}$, which are the same for Zn01 and Zn02, reveal that the metal−metal distances within the octahedral sheet do not depend on the Zn content in montmorillonite. However, the amplitude of the Zn contribution is enhanced by a factor of about one third in Zn02 with respect to Zn01. Coming back to the Si and Al contributions, the differences observed between Zn01 and Zn02, around 3−8 $Å^{-1}$, are attributed to a variation of the distance from Zn to Si(Al) belonging to the tetrahedral sheets. Following these considerations, the fits were performed by keeping the number of Si(Al) that are underneath and beyond the Zn, located in the plane of the octahedral sheet, constant and equal to four. The number of metallic neighbours inside the octahedral sheet was also kept constant and equal to four. The preferential orientation of the crystallites has not been considered in this preliminary treatment of the Zn k-edge data. An accurate determination of the absolute coordination numbers requires a careful texture analysis which has not yet been carried out.[31] Consequently, only an evaluation of the N_{Zn}/N_{Al} ratio can be deduced from the data treatment at this stage. After the interatomic distances and Debye−Waller parameters were roughly determined (with initial values of the Al and Zn coordination numbers taken to be 3 and 1, respectively) the Al/Zn ratio was varied step by step until the lowest value of the residue was obtained. In the octahedral sheet, the Zn−Al and Zn−Zn distances are found to be 2.98 and 3.11 Å for Zn01 and Zn02, respectively (Table 4). The values of 2.0 and 2.3 Zn neighbours of Zn are consistent with the amplitude of the data in the high k-range. The Zn−Si(Al) distances are found to be 3.17 and 3.25 Å in Zn01 and Zn02, respectively. The latter value is longer than the mean Al−Si distance in the ideal structure (3.15 Å). This main result clearly demonstrates that the montmorillonite lattice is submitted to more and more distortions as the Zn content is increased.

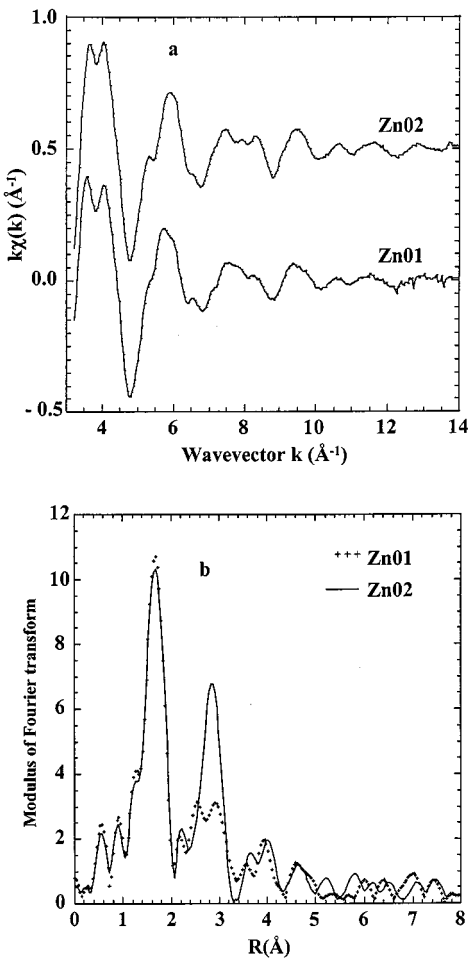

Figure 9. EXAFS data (a) and RDF (b) of synthetic montmorillonites containing Zn (samples Zn01 and Zn02)

The Mg k-edge spectra of samples Mg01 and Mg02 are presented in Figure 11a and the corresponding FT in Figure 11b. The results of the fits give a value of the Mg−O distance of 2.11 Å (Table 5) similar to the Zn−O distance.

Table 4. Structural parameters derived from Zn *K*-edge EXAFS analysis

	Sample	Shell	*N*	*R* [Å]	σ^2 [Å^2]
NN shell	Zn01	Zn−O	5.9	2.08±0.02	0.004
	Zn02	Zn−O	5.9	2.07±0.02	0.004
		Zn−Al	2.0[a]	2.98±0.04	0.007
	Zn01	Zn−Zn	2.0[a]	3.11±0.04	0.005
NNN shell		Zn−Si	4.0[b]	3.17±0.04	0.005
		Zn−Al	1.7[a]	2.97±0.04	0.006
	Zn02	Zn−Zn	2.3[a]	3.11±0.04	0.006
		Zn−Si	4.0[b]	3.25±0.04	0.005[b]

[a] The sum of N_{Zn-Al} and N_{Zn-Zn} was fixed to 4.0. − [b] Fixed parameter.

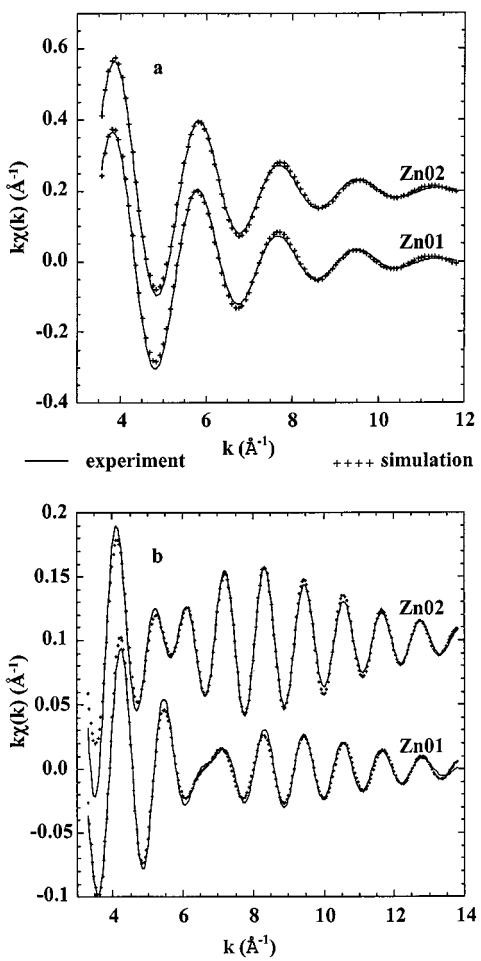

Figure 10. Best fits performed on the Fourier-filtered NN shell (a) and NNN shell (b) contributions using the parameters reported in Table 2: samples Zn01 and Zn02

Due to the short-range data (2−8 Å^{-1}) the NNN shell has not yet been investigated.

Discussion

XRD and ^{29}Si MAS NMR spectroscopic studies of the $MgO-Al_2O_3-SiO_2$ and $ZnO-Al_2O_3-SiO_2$ systems demonstrate that montmorillonite can only be synthesized in a narrow range of compositions ($x = 0.2$). The XRD patterns of Mg01, Mg02, Zn01, and Zn02 selected samples (Figure 3) are unambiguously assigned to smectites and exhibit the typical *hkl* bands of montmorillonite.[12] Moreover, the morphology of the crystal particles observed by SEM (Figure 4) are similar to those of natural montmorillonites.[16−18]

The TGA-DTA analysis (Figure 5), which gives information about the octahedral sheet, confirms this result since the dehydroxylation peak characteristic of natural montmorillonite is observed between 920 and 960 K.[19−23] The additional dehydroxylation peak, which appears in the 720−760 K range, was assigned by Cuadros et al. to the presence of kaolinite.[20] However, the characteristic exothermic contribution of kaolinite above 1173 K is not ob-

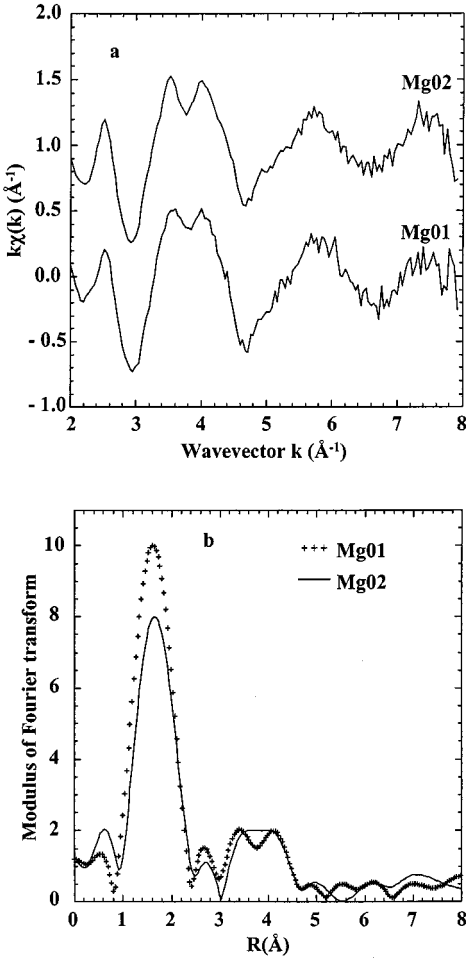

Figure 11. EXAFS data (a) and RDF (b) of synthetic montmorillonites containing Mg (samples Mg01 and Mg02)

Table 5. Structural parameters derived from Mg *K*-edge EXAFS analysis

	Sample	Shell	*N*	*R* [Å]	σ^2 [Å^2]
NN shell	Mg01	Mg−O	6	2.12±0.02	0.006
	Mg02		6	2.10±0.02	0.007

served for the four synthetic clays.[32] On the other hand, the endothermic peak observed at 720−760 K cannot be assigned to the presence of a small amount of kaolinite, because the typical endothermic contribution of kaolinite appears at higher temperatures.[20] The endothermic peak observed in our case (Figure 5) is attributed to hydroxy groups which have different octahedral metallic neighbours. In this way, Frost et al. have assigned the low-temperature dehydroxylation endotherm of a ferruginous montmorillonite to hydroxy groups associated with Fe−Fe pairs and the higher one to hydroxy neighbour Fe−Al pairs.[23] Therefore, the presence of extraneous kaolinite can be ruled out in the four analysed synthetic montmorillonites. The deviation of a random distribution of metallic atoms inside the montmorillonite lattice will be discussed below.

Both ^{29}Si and ^{27}Al MAS NMR spectroscopy gave proof that Al is partially substituted for Si in the tetrahedral sheets. Chemical analysis is not accurate enough to probe such a kind of substitution. It appears that whatever the synthetic conditions, the incorporation of small amounts of aluminium in the tetrahedral sheet (Al_{IV}) cannot be avoided. The Si/Al_{IV} ratio could not be determined by ^{29}Si MAS NMR spectroscopy because of the deviation of the statistic distribution pointed out below. Sanz and Serratosa have indeed shown that other factors exist besides the rule of Loewenstein (no Al−O−Al bond in the structure), which governs the Si and Al distribution in the tetrahedral sheet, when atoms are not randomly distributed in the layer.[24] Working on natural pyrophyllite (talc-type clay), muscovite and margarite (mica-type clays) as dioctahedral clays which have only tetrahedral substitutions, Sanz and Serratosa have reported a poor agreement between the Al_{VI}/Al_{IV} ratio determined by using ^{27}Al MAS NMR spectroscopy and those calculated from the chemical analysis and ^{29}Si MAS NMR spectroscopy.[26] Later, Goodman and Stucki noticed that ^{27}Al MAS NMR spectroscopy can be used to obtain the Al_{VI}/Al_{IV} ratio and probably, in precise experimental conditions, have accurate quantitative results in the case of natural montmorillonite.[28] The presence of paramagnetic elements in the samples of Sanz and Serratosa and the fact that the spinning rate was lower for the MAS at this time, could explain the poor agreement for ^{27}Al MAS NMR spectroscopy in their study.[24] Nowadays, the knowledge about ^{27}Al MAS NMR spectroscopic technology has improved, particularly that concerning the quantitative analysis.[33−35] The determination of the absolute Al contents in Mg01, Mg02, Zn01, and Zn02 by ^{27}Al MAS NMR spectroscopy can now be achieved. The calibration was made using well-known synthetic beidellites.[9,10] However, the determination of the Al_{VI}/Al_{IV} ratio by this technique requires complementary measurements that are currently in progress.[36]

The EXAFS study provides a determination of the NN and NNN shell distances. NN shell distances are very similar for samples Zn01 and Zn02 (2.08 Å and 2.07 Å, respectively) and for samples Mg01 and Mg02 (2.12 Å and 2.10 Å, respectively). These values have to be compared to those of an ideal montmorillonite lattice, where two types of octahedral sites exist: the first one, here called M_1, and the second one called M_2.[29] Only the M_2 octahedral site is occupied by an atom and the value of the M_2−O distance is 1.94 Å. These deviations indicate a strong distortion of the coordination polyhedron with respect to the ideal structure. In the case of the NNN shell, the values of the out-of-plane Zn−Si distance increases with the quantity of Zn contained in the octahedral sheet (3.17 Å for Zn01 and 3.25 Å for Zn02, as a comparison d_{M-Si} = 3.15 Å in the ideal lattice). The values of the Zn−Al distance deduced for samples Zn01 and Zn02 (2.98 Å and 2.97 Å, respectively) are close to those of the ideal montmorillonite lattice (2.99 Å), whereas the values deduced for the Zn−Zn distance are longer (3.11 Å for both Zn01 and Zn02). This observation confirms that the distance between two elements in the structure strongly depends on their nature.

Finally, let us consider the distribution of tri- and divalent elements within the octahedral sheet. The simulation of the backscattered contribution of the NNN of Zn reveals a surprisingly high value of the Zn/Al_{VI} ratio, which reaches 1.0/1.0 in Zn01 and 1.4/1.0 in Zn02 (Table 4). The projection of the octahedral sheet onto the (*ab*) plane has the form of a two-dimensional hexagonal network whose every third apex is vacant (Figure 1b). If we consider various arrangements of vacancies within this plane, the average coordination number of an element is four (at least 3, at most 5). Consequently, the coordination number of Zn was kept constant and equal to 4 in the simulations. The value of the octahedral substitution, which could be determined by using ^{27}Al MAS NMR spectroscopy and chemical analyses, indicates 1.8 Al for 0.2 Zn in Zn01 and 1.6 Al for 0.4 Zn in Zn02, i.e. one octahedral site out of 15 and two octahedral sites out of 15 are occupied by Zn atoms in Zn01 and Zn02, respectively. For a random distribution of the elements in the sheet, the number of Zn neighbours of Zn would be much less than one in both Zn01 and Zn02. On the other hand, the TGA-DTA study has also demonstrated a possible deviation from a random distribution of metallic atoms inside the montmorillonite lattice. The deviation from the statistical distribution and the clustering of divalent elements is also confirmed by ^{19}F MAS NMR spectroscopy that reveals unambiguously the presence of Mg−Mg−Mg arrangement around fluorine atoms in the Mg02 sample. The existence of a Mg−Mg−Mg environment and the absence of a Zn−Zn−Zn one could also be explained by a higher affinity of fluorine for Mg than Al or Zn due to the difference between the electronegativity of the elements. The clustering induces strong local distortions within the octahedral sheet that are balanced by the tetrahedral sheet substitutions. This behaviour was already observed in the octahedral sheet of a natural montmorillonite from Camp Berteau by EXAFS measurements at the Ni *k*-edge.[37]

Conclusion

Montmorillonites containing Al and exclusively Zn or Mg as divalent elements in the octahedral sheet were syn-

thesized in acidic and fluoride medium. The substitution of Al in the octahedral sheet was obtained for a narrow range of Mg or Zn contents. The elemental analysis (XRD, TGA-DTA, chemical analysis) of the synthesized materials demonstrates their major dioctahedral character. Beyond these fundamental characterisations, ^{27}Al MAS NMR spectroscopy gives an accurate value of the substitution rate of the Al for Si in the tetrahedral sheet and demonstrates that elemental analyses are not sufficient to establish the half unit cell formula. EXAFS reveals substantial increases of the bond lengths (R_{Mg-O} = 2.11 Å, R_{Zn-O} = 2.08 Å, R_{Zn-Al} = 2.98 Å, R_{Zn-Zn} = 3.11 Å) in the octahedral sheet with respect to the ideal structure. The distortions of the coordination polyhedra of divalent elements could be related to a local trioctahedral character of these materials. This interpretation can be connected with the clustering of divalent elements revealed by EXAFS and ^{19}F MAS NMR spectroscopy. It appears that the substitution and the clustering of the divalent elements induce a mismatch between the octahedral and the tetrahedral sheets, and finally a local undulation of the layer which could be compensated by Al for Si substitutions in the tetrahedral sheet. This could be the reason why montmorillonite clays without tetrahedral substitutions are seldom observed in nature. The relevant phenomena may influence the physical and the chemical properties of these clays (adsorption, catalytic efficiency, etc.).

Experimental Section

Synthesis: Two series of syntheses were performed on $MgO-Al_2O_3-SiO_2$ and $ZnO-Al_2O_3-SiO_2$ systems. The compositions of hydrogel are based on a theoretical formula of montmorillonite: $Na_{2x}[(Al_{2(1-x)}M_{2x}\ \square)Si_4O_{10}(OH,F)_2]\cdot nH_2O$. M represents the divalent element (Mg or Zn), and x ranges from 0.0 to 1.0. Samples were synthesized in an acidic fluoride medium under hydrothermal conditions using hydrogels with the following molar composition:

$$1SiO_2 : (1 - x)/4\cdot Al_2O_3 : x/2\cdot MO : x/4\cdot Na_2O : 0.05\cdot HF : 96\cdot H_2O$$

Water, hydrofluoric acid, and silicon oxide contents are the same for each synthesis. Reactants were mixed in the following order: deionized water, hydrofluoric acid (HF, 40%; BDH), sodium acetate ($NaCOOCH_3$, 99%; Fluka), zinc acetate [$Zn(COOCH_3)_2$, $2H_2O$, 98%; Prolabo] or magnesium acetate [$Mg(COOCH_3)_2\ 4H_2O$, 99%; Fluka], boehmite (Al_2O_3, 75−78%, Pural SB1; Condea), and silica (SiO_2, 99.5%, Aerosil 130; Degussa). Hydrogels were matured over 2 h at room temperature and the pH was measured (pH = 4.5−6) before hydrothermal treatment in a PTFE-lined stainless steel autoclave at 493 K for 72 h under autogeneous water pressure. After crystallisation, the autoclaves were cooled to room temperature. The pH of the supernatant was 3.5−4.5. Products were then separated by filtration, washed thoroughly with distilled water and dried at 333 K for 12 h. The samples were then ground to a fine powder form and placed under controlled humidity. This was made by keeping samples under a relative pressure P/P_0 = 80%, by using a saturated solution of NH_4Cl salt.

X-ray Powder Diffraction (XRD): The X-ray powder diffraction patterns were recorded with two diffractometers: the first one employing Cu-K_α radiation was equipped with automatic divergence slits (Philips PW1800), the second one employing either Cu-K_α or Cr-K_α radiation with fixed divergence slits (Philips PW1100). The latter enables patterns to be recorded under controlled humidity (P/P_0 = 80% RH). In both cases diffractograms were performed on powders which were only pressed on sample carriers. Information about the phase and d_{001} spacing was obtained with the APD 1700 software (Philips).

Scanning Electronic Microscopy (SEM): Starting materials were first examined by SEM with a Philips XL30 microscope in order to determine their morphology. An ethanolic suspension of the sample was left on a support covered by graphite and then evaporated. Samples were then metallized (10 or 20 nm of gold) under vacuum by sputtering.

Thermal Analysis (TGA-DTA): Measurements were carried out on samples which were previously placed under controlled humidity (P/P_0 = 80%), with a heating rate of 5 K·min^{-1} obtained by using a Setaram Labsys apparatus under a mixture of N_2 and O_2 (1 and 0.5 bars, respectively).

Chemical Analysis: A part of each sample was Na-saturated to be sure that only Na^+ cations balanced the charge. Na-saturated products were prepared as follows: 5 mL of 1 M NaCl solution was added to 0.5 g of synthetic product. The mixture was stirred at room temperature for 1 h before it was filtered. The exchange process was repeated twice. The samples were then washed with distilled water until the product was chloride-free (this was tested using $AgNO_3$ solution). The resultant product was then dried at 333 K for 12 h. Elemental analysis of Na-saturated clays was then performed by the Service Central d'Analyse of the Centre National de la Recherche Scientifique (Vernaison, France) for the following elements: Mg, Zn, Al, Si, and F.

Solid-State Nuclear Magnetic Resonance (NMR) Spectroscopy

Experiments: ^{29}Si MAS NMR spectra were obtained with a Bruker MSL-300 spectrometer at 59.63 MHz with 4 kHz spinning speed, 2 μs excitation pulses (π/2 pulse width of 4 μs) and 95 s recycle time. Chemical shifts of Si were referenced to tetramethylsilane (TMS) using a secondary standard of trimethylsilyl ester of cubic octameric silicate (Q8M8) at δ = −109.7 (the more shielded signal). ^{27}Al MAS NMR spectra were obtained with a Bruker MSL-300 spectrometer at 78.21 MHz with 10 kHz spinning speed, 0.7 μs excitation pulses (π/2 pulse width of 9 μs for an aqueous solution) and 1 s recycle time. Chemical shifts of aluminium were referenced to a 1 M $Al(NO_3)_3$ aqueous solution with a chemical shift of δ = 0. ^{19}F MAS NMR spectra were obtained with a Bruker DSX-400 spectrometer at 379.23 MHz with a Hahn echo pulse sequence (π/2 pulse − τ − π pulse − τ − acquisition),[38] 10 kHz spinning speed, π/2 pulse width of 7 μs and 20 s recycle time.

Data Analysis: After their collection, free-induction decay (FID) signals were treated following a standard procedure using the software WIN NMR (Bruker software). The FID signals were smoothed in order to reduce the background noise. Base-lines were also corrected when necessary. The ^{29}Si MAS NMR spectra were simulated with the WINFIT software.[39] The Al_{VI}/Al_{IV} ratio was calculated by determining the area of each component of the ^{27}Al MAS NMR spectra. Furthermore, the aluminium content was determined accurately by using quantitative ^{27}Al MAS NMR spectroscopic conditions.[33−36]

Extended X-ray Absorption Fine Structure (EXAFS)

Experiments: The X-ray absorption experiments were performed at the Laboratoire pour l'Utilisation du Rayonnement Electromagnétique (LURE, Orsay, France). Samples studied by EXAFS were named Mg01, Mg02, Zn01, and Zn02, see below for their selection. The Zn01 and Zn02 samples were mixed with cellulose (0.122 g of Zn01 and 0.006 g of cellulose, 0.121 g of Zn02 and 0.005 g of cellulose), and pressed (1 T and 1.5 T, respectively) in the form of pellets (less than 1 mm thickness), that were maintained between two Kapton windows. Measurements were performed on the D21 beam line of the DCI storage ring. The X-rays were monochromatized by an Si(311) two-crystal spectrometer. The X-ray absorption spectra were recorded at the Zn-*K* edge (9659 eV) from 9400 to 10900 eV (1 eV step; 1 s^{-1} per point) in transmission mode at 20 K. Measurements for the Mg (1305 eV) and Al (1559 eV) *K* edges were performed on the SA32 beam line of the Super−Aco storage ring. Powdered Mg01, Mg02, Zn01, and Zn02 samples were directly pressed on indium films deposited on a copper sheet used as a support. The X-ray absorption spectra were collected at the Mg-*K* edge between 1250 and 1560 eV (1 eV step; 4 s^{-1} per point) in fluorescence mode. X-rays were monochromatized by a spectrometer using beryl crystals. All the spectra were collected with the samples perpendicular to the beam path. Measurements were performed at room temperature in a chamber at a pressure of 10^{-9} bar.

Data Analysis: The raw data were analysed following the standard procedure by using the software designed by Michalowiz.[40] First the pre-edge and post-edge backgrounds were removed from the raw data. After conversion to *k*-space, the EXAFS spectra were k^3-weighted and Fourier-transformed using a Kaiser apodization window. The nearest neighbours (NN) and next-nearest neighbours (NNN) peaks in the Fourier transforms (FT) were assigned to the oxygen and metal backscatterers. The Fourier-filtered (FF) contribution of oxygen was simulated using a squares fit by the standard EXAFS formula in order to derive the structural parameters: the interatomic distances *R*, coordination numbers *N* and Debye−Waller (DW) parameters σ. The amplitude and phase shifts are extracted either from reference samples or theoretical calculation.[30] The Fourier-filtered contribution of the metallic NNN of Zn in the 2.0−3.3 Å range (Figure 9 b) were simulated with amplitude and phase shifts calculated by using the FEFF software.[30]

Acknowledgments

The authors are grateful to Jean-Marc Le Meins for the interesting and helpful discussions concerning crystallography and for providing Figure 1. We also thank Anne-Catherine Faust for SEM micrographs.

[1] M. Ogawa, K. Kuroda, *Chem. Rev.* **1995**, *95*, 399−438.
[2] F. Figueras, *Catal. Rev. Sci. Eng.* **1988**, *30*, 457−499.
[3] A. Clearfield, *Chem. Mater.* **1998**, *10*, 2801−2810.
[4] J. T. Kloprogge, S. Komarneni, J. E. Amonette, *Clays Clay Miner.* **1999**, *47*, 529−554,
[5] Y. Otsubo, C. Kato, *J. Chem. Soc. Jpn.* **1954**, *75*, 456−459,
[6] H. Harder, *Chem. Geol.* **1972**, *10*, 31−39,
[7] H. Nakazawa, H. Yamada, K. Yoshioka, M. Adachi, T. Fujita, *Clay Sci.* **1991**, *8*, 59−68,
[8] T. Nagase, T. Iwasaki, T. Ebina, H. Hayashi, Y. Onodera Chandra, N. Dutta, *Chem. Lett.* **1999**, *4*, 303−304,
[9] L. Huve, L. Delmotte, R. Le Dred, J. Baron, D. Saehr, *Proc. ACS Symposium on Advances in Zeolites and Pillared Clays Synthesis*, New York, **1991**.
[10] J.-F. Joly, L. Huve, R. Le Dred, D. Saehr, J. Baron, French patent no. 2673930, **1992**.
[11] F. Lhommédé, R. Le Dred, D. Saehr, J. Baron, *C. R. Acad. Sci. Paris* **1996**, *t. 322 série Iia*, 827−830.
[12] E. Maegdefrau, U. Hofmann, *Z. Kristallogr.* **1937**, *98*, 299−323.
[13] T. Watanabe, T. Sato, *Clay Sci.* **1988**, *7*, 129−138.
[14] H. Yamada, H. Nakazawa, H. Hashizume, S. Shimomura, T. Watanabe, *Clays Clay Miner.* **1994**, *42*, 77−80.
[15] E. S. Boeck, P. V. Coveney, N. T. Skipper, *J. Am. Chem. Soc.* **1995**, *117*, 12608−12617.
[16] S. P. Skaribas, P. J. Pomonis, P. Grange, B. Delmon, *Multifunctional Mesoporous Inorganic Solids* (Eds.: C. A. C. Sequeira, M. J. Hudson), Kluwer Academic Publishers, Netherlands, **1993**, p. 127−136.
[17] K. Ma, A. C. Pierre, *Colloid Surface A* **1999**, *155*, 359−372.
[18] F. Cravero, K. S. Keith, H. H. Murray, T. Toth, *Appl. Clay Sci.* **2000**, *16*, 31−43.
[19] R. Greene-Kelly, *Clay Min. Bull.* **1952**, *1*, 221−225.
[20] J. Cuadros, A. Delgado, A. Cardenete, E. Reyes, J. Linares, *Clays Clay Miner.* **1994**, *42*, 643−651.
[21] A. Garcia-Rodriguez, F. del Rey-Bueno, F. J. del Rey-Perez-Caballero, M. D. Ureña-Amate, A. Mata-Arjona, *Mater. Chem. Phys.* **1995**, *39*, 269−277.
[22] M. D. Alba, R. Alvero, A. I. Beccero, M. A. Castro, J. M. Trillo, *J. Phys. Chem. B* **1998**, *102*, 2207−2213.
[23] R. L. Frost, H. Ruan, J. T. Kloprogge, W. P. Gates, *Thermochim. Acta* **2000**, *346*, 63−72.
[24] J. Sanz, J. M. Serratosa, *J. Am. Chem. Soc.* **1984**, *106*, 4790−4793.
[25] S. R. Drachman, G. E. Roch, M. E. Smith, *Solid State Nucl. Magn.* **1997**, *9*, 257−267.
[26] G. Engelhardt, D. Michel, *High resolution solid- state NMR of silicates and zeolites*, J. Wiley & Sons, New York, **1987**, p. 129.
[27] L. Huve, L. Delmotte, P. Martin, R. Le Dred, J. Baron, D. Saehr, *Clays Clay Miner.* **1992**, *40*, 186−191.
[28] B. A. Goodman, J. W. Stucki, *Clay Miner.* **1984**, *19*, 663−667.
[29] S. I. Tsipursky, V. A. Drits, *Clay Miner.* **1984**, *19*, 177−193.
[30] J. J. Rehr, J. Mustre de Leon, S. I. Zabinsky, R. C. Albers, *J. Am. Chem. Soc.* **1991**, *113*, 5135−5145.
[31] A. Manceau, D. Chateigner, W. P. Gates, *Phys. Chem. Miner.* **1998**, *25*, 347−365.
[32] G. Suraj, C. S. P. Iyer, S. Rugmini, M. Lalithambika, *Appl. Clay Sci.* **1997**, *12*, 111−130.
[33] D. Plee, F. Borg, L. Gatineau, J. J. Fripiat, *J. Am. Chem. Soc.* **1985**, *107*, 2362−2369
[34] A. Samoson, E. Lippma, G. Engelhardt, U. Lohse, H.-G. Jerschkewitz, *Chem. Phys. Lett.* **1987**, *134*, 589−592.
[35] N. C. Nielsen, H. Bildsøe, H. J. Jakobsen, *Chem. Phys. Lett.* **1992**, *191*, 205−212.
[36] M. Reinholdt, J. Miehé-Brendlé, L. Delmotte, M.-H. Tuilier, R. Le Dred, to be published.
[37] F. Muller, G. Besson, A. Manceau, V.-A. Drits, *Phys. Chem. Miner.* **1997**, *24*, 159−166.
[38] E. L. Hahn, *Phy. Rev.* **1950**, *80*, 580−594.
[39] D. Massiot, *Winfit 990420 version*, Centre de Recherches sur les Matériaux à Haute Température, Orléans, http://crmht.cnrs-orleans.fr/Pole2/ThemeDM/default.htm
[40] A. Michalowiz, *J. Phys.* **1997**, *III − C2*, 235−237.

Received April 23, 2001
[I01143]